On Simulating the Effect of Sodium Channel Block on Cardiac Electromechanics

Noha Shalaby, Nejib Zemzemi, Khalil Elkhodary

On Simulating the Effect of Sodium Channel Block on Cardiac Electromechanics

Noha Shalaby[1,*], Nejib Zemzemi[2,3], Khalil Elkhodary[1]

Abstract— *Objective:* The purpose of this paper is to investigate computationally the influence of sodium ion channel block on cardiac electro-mechanics. *Methods:* To do so, we implement a myofiber orientation dependent passive stress model (Holzapfel-Ogden) in the multiphysics solver Chaste to simulate an imaged physiological model of the human ventricles. A dosage of a sodium channel blocker was then applied and its inhibitory effects on the electrical propagation across ventricles modeled. We employ the Kirchhoff active stress model to generate electrically excited contractile behavior of myofibers. *Results:* Our predictions indicate that a delay in the electrical activation of ventricular tissue caused by the sodium channel block translates to a delay in the mechanical biomarkers that were investigated. Moreover, sodium channel block was found to increase left ventricular twist. *Conclusion:* A multiphysics computational framework from the cell level to the organ level was used to predict the effect of sodium channel blocking drugs on cardiac electromechanics. *Significance:* There is growing interest to better understand drug-induced cardiovascular complications and to predict undesirable side effects at as early a stage in the drug development process as possible.

---

* Corresponding author. Email: nohasamyshalaby@aucegypt.edu
1. The Mechanical Engineering Department, The American University in Cairo, Egypt
2. INRIA Bordeaux Sud-Ouest, Carmen Group, France
3. IHU-LIRYC, Pessac France

Keywords— Cardiac electromechanics; computational modeling; finite element modeling; continuum mechanics; drug; ion channel block

1 Introduction

Cardiac muscle cells, or *myocytes*, are among a class known as *excitable cells*. That is, they actively respond to an incident electrical stimulus that induces a flow of ions across the cell membrane, which ultimately results in myocytes contraction associated with a heartbeat. Specifically, ions of sodium (Na^+), potassium (K^+) and calcium (Ca^{2+}) naturally flow through cardiac cell trans-membrane ion channels, for normal cardiac behavior to arise (1). However, when chemicals or drugs are administered, they often interact with these ion channels and partial or full inhibition to ionic flow could result, disrupting the electrophysiology and mechanical function of the heart (2). In fact, one of the foremost reasons for drug discontinuation at all phases of their development is *cardiotoxicity*, in both cardiac and non-cardiac pharmaceuticals (3). Cardiotoxicity can be defined as the occurrence of an electrophysiological dysfunction of the heart or a mechanical abnormality of cardiac muscular behavior as a result of the intake of toxic matter (4). Cardiovascular safety concerns have been responsible for almost 19% of drug

withdrawals in the United States alone, over the past 40 years and for 9% of worldwide withdrawals (3).

Drug development and approval takes extensive time, money and effort and is subject to high failure rates (3). In fact, many promising drugs pass the initial cytotoxicity (toxic to regular cells) screening only to turn out to be highly cardiotoxic in preclinical trials (5). Often, adverse drug effects on cardiac function appear only after completion of clinical trials, or after drug release in the market (6). Detecting adverse drug interactions at such a late stage could undoubtedly cause a negative impact on public health. Thus, there is growing interest to better understand drug-induced cardiovascular complications and to predict undesirable side effects at as early a stage in the drug development process as possible.

To minimize potential risks from cardiotoxicity, much research has been directed towards the development of accurate cardiac *modeling and simulation* platforms, as an increasingly popular supplement to clinical and experimental (in-vitro) studies on the human heart. Modeling and simulation, or *in-silico* testing, promises a new *predictive* capability of clinical biomarkers, for the rigorous evaluation of cardiotoxicity. In-silico methods are especially sought for, due to their greater safety and their ability to shed light on the basic underlying phenomena, which arise from the chemistry, biology, electrophysiology and mechanics of the heart (7).

In recent years, various models have been put forward to relate drug effects to cardiac electrophysiology and these models are rapidly growing in sophistication; having evolved from single cell predictions, to large scale models embedded in the torso, to even whole-body geometries with body surface potentials, where drug-induced single and multiple channel blocks can be recorded, analyzed and compared (8–12). Recently, these advanced electro-physiological models have been integrated with cardiac mechanics simulators, within a *multiphysics* computational framework. Several studies have thus been published, aiming to capture the interactions that characterize human cardiac electromechanics, from the cell levels to the organ level (*multiscale*) (7,13,14). Some studies are now focused on building a model for the complex fiber orientation of the cardiac walls, in order to properly capture that rotation and twist of the left ventricle (LV) and use the quantification and interpretation of LV torsion as a potential tool of clinical relevance (15,16). Other models aim to develop the most accurate material law describing the mechanical properties of cardiac tissue, both active and passive (with respect to electrical excitation) and to accurately predict corresponding stresses, strains and volume change from cardiac contraction (17,18).

Such advances in electromechanical models are increasing their readiness for application in the treatment of cardiac disease, by better poising them to reproduce the effects of various pathologies, simulating full surgical interventions, predicting relevant stress and strain fields and quantifying changes in tissue material parameters (19). Nevertheless, linking these state-of-the-art electromechanical methods to drugs and the assessment of drug safety has not taken root (20).

This points to a fertile ground for a computational multiphysics exploration, to lend a reliable hand to the safe advancement of drug development.

It is thus the objective of this work to investigate the drug-induced effect of Na^+ channel blockage on cardiac electro-mechano-physiology, by implementing and integrating an improved model of (passive) cardiac myofiber mechanics in a suitable multiphysics framework that couples directly to the applied drug dosage. Specifically, in this paper an imaged physiological model of the human ventricles (21,22) is studied by the finite element method, on the multiphysics solver *Chaste* (Cancer, Heart and Soft Tissue Environment) (23,24). Chaste is an open source software package that presently integrates nanoscale ionic flow from myocytic currents with macroscale electrical propagation across ventricular tissue and contractile tissue behavior (active and passive), to accurately predict associated electrical and mechanical biomarkers of the heart. However, Chaste presently features two rather restrictive (passive) material laws to describe cardiac tissue electro-mechanics. As such, an improved (passive) material law was herein implemented, based on the work of Holzapfel and Ogden (18) then used in the analysis of Na^+ channel blocking drug-induced effects.

2 Methodology

Electrophysiology

To model the flux of ions and associated electrical activity of an individual myocyte in humans, the Ten Tusscher and Panfilov (TP06) action potential model (25) is used. TP06 combines the 15 major ionic channels that allow the flow of Na^+, K^+ and Ca^{2+} ions in and out of the human ventricular cardiac myocyte. It is one of the most widely used ionic models in the literature (8,11,12,26) and has thus been verified as an efficient model that produces reliable results which relate well to experimental data (27,28). The following conductance formula is used to model the inhibitory effect of a specific drug dosage on the ionic channels, by setting the Hill coefficient $n = 1$ (10,11),

$$g_j([D]) = g_j\left(\frac{1}{1+\left(\frac{[D]}{IC_{50}}\right)^n}\right) \quad [1]$$

By equation [1], the degree of an ionic channel blockage is dependent on the dosage [D] and the IC_{50} (half-maximal inhibition) of the investigated drug, assumed known a priori. Index j labels the targeted ion channel of a myocyte, which in this work will be Na^+.

Using the altered ionic channel conductance from [1], the sum of all the trans-membrane ionic currents (I_{ion}) is computed from TP06. The resultant current is then passed to the monodomain reaction-diffusion equation, which characterizes the propagation of electrical activity across the cardiac domain (29). It is less computationally intensive than the bidomain model and gives sufficiently accurate results with respect to electrical propagation and ionic channel blocking (30). The governing monodomain equation can be expressed as:

$$\chi \frac{\partial V_m}{\partial t} = \nabla . (D_M \nabla V_m) - \frac{\chi I_{ion} + I_{applied}}{C_m} \quad [2]$$

where χ is the surface-area-to-volume ratio, V_m is the trans-membrane voltage, t is the time, C_m is the capacitance across the membrane, $I_{applied}$ is the applied stimulus and I_{ion} is the value passed on from the TP06 ionic model, representing the sum of all the trans-membrane ionic currents. D_M is the effective conductance tensor expressing the anisotropic electrical properties of the cardiac tissue.

Hence, once an external electrical stimulus is applied to cardiac tissue, a corresponding change in trans-membrane potential is communicated from the monodomain equation [2] to the TP06 ionic model, to solve for the associated ionic flow through myocyte channels and update calcium and other ionic concentration as state variables. The resulting TP06 ionic current is then fed back to the monodomain equation, which updates cell membrane voltage, thus providing for a two-way coupling scheme between myocyte chemistry and cardiac electrophysiology. For further details on the electrophysiological model used herein, the reader is referred to (31).

Tissue Mechanics

The heart has a complex structure; one composed of a multitude of myofibers that follow different orientations across the cardiac domain, and which are crucial in defining directional electrical propagation (21) and mechanical contraction of the heart (32). In the ventricles, myofibers evolve continuously from a right-handed helix in the sub-endocardium to a left-handed helix in the sub-epicardium. Such reversal in myofiber orientation induces complex contraction patterns across the ventricular wall. The larger radius associated with the outer wall layers permits them to dictate the final direction of ventricular rotation and its overall twisting pattern. The opposing orientation of myofibers in the endocardium magnify shearing strains throughout the cardiac wall and amplify strain energy storage in the contraction phase that serves for diastolic recoil (33).

Cardiac tissue mechanics is thus strongly dependent on the non-uniform alignment of myofibers across the cardiac domain. Indeed, models of the ventricles that have not captured myofiber orientation lead to incorrect distributions of strain (and stress), a decrease in cardiac energy efficiency and an overall compromise in the accuracy of the predicted cardiac electromechanical phenomena (33,34). To properly account for myofiber orientation, therefore, models have been put forward for single myofiber mechanics in its natural coordinates and then generalized to accommodate arbitrary orientations.

In particular, in its natural orientation, each myofiber may be seen to be composed of a multitude of parallel *myofibrils*, each myofibril being built up in series by cylindrical sarcomeres. An electrical excitation of the sarcomeres releases active forces, which induce collective myofiber contraction and/or relaxation while following the force-extension curves depicted in

Figure 1. Maximum active force is produced when a sarcomere is at its intermediate length (b, c, d), while no active force results at either extreme of sarcomere length (a, e). On the other hand, a passive force may be present in the myocyte, irrespective of electrical excitation, due to the (nonlinear) elasticity of its connecting filaments and the collagen surrounding each myofiber. The mechanisms of active and passive force generation are thus independent. Hence, it is typical to model active and passive forces (or stresses) as superimposed (additive) as indicated in Figure 1 (35).

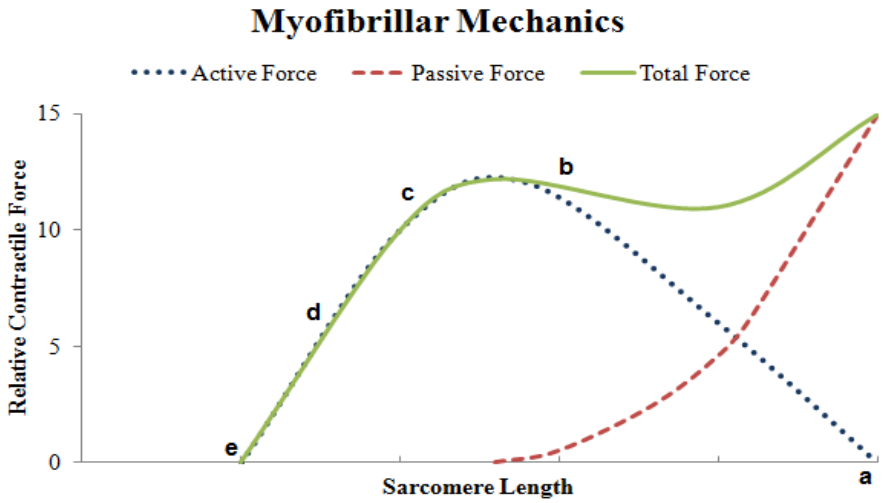

Figure 1: Total contractile force developed during contraction generated by active and passive forces.

Within this framework, the active response to electrical excitation is herein defined via the second *Piola-Kirchhoff* (PK2) stress tensor, $\mathbf{T}_a$, whose tensorial form will render the active stress orientation dependent. In particular, the *Kirchhoff* model is used to simulate the parabolic behavior shown in Figure 1. Its predictions depend on the time elapsed since electrical depolarization and some mechanical properties of the contracting myofibers (36). We adopt its use for its comparative numerical stability, computational efficiency and its ability to capture the effect of Na^+ channel block. The active PK2 stress may thus be written as (31),

$$\mathbf{T}_a = \frac{J\sigma_a}{\lambda^2}\mathbf{f}_0 \otimes \mathbf{f}_0 \qquad [3]$$

In equation [3], J is the determinant of the deformation gradient $\mathbf{F}$ and $\mathbf{f}_0$ is the fiber orientation vector referred to the initial configuration of the ventricles. σ_a is the coefficient of active Cauchy stress (31) , and λ is the stretch experienced by the deforming myofiber.

As for the passive stress, hyperelasticity is assumed (18,37). Viscoelastic and poroelastic effects are thus ignored and the myofiber is deemed incompressible. An isochoric strain energy function is thus introduced (38);

$$W_{\text{iso}} = W(\mathbf{u}) - p(I_3 - 1) \qquad [4]$$

In equation [4], p is a Lagrange multiplier, interpreted as a hydrostatic pressure that penalizes any volume change while enforcing isochoric deformation. I_3 is the third invariant of the right Cauchy-Green strain $\mathbf{C}$. $W(\mathbf{u})$ is a strain energy density function of displacement gradient $\mathbf{u}$, which describes the passive response to both volumetric and isochoric deformation.

On Chaste, there are two alternative definitions for $W(\mathbf{u})$ for cardiac electro-mechanics. The first stems from the work of Mooney (39) and Rivlin (40) on the large elastic deformation of rubber-like isotropic materials. The second model is due to Nash and Hunter (17). It involves a transversely isotropic material law, calibrated against biaxial tests that were performed on thin sections of passive myocardium tissue. These models have been found to give weaker predictions of ventricular volume change and ejection fraction than the Holzapfel and Ogden (18) implemented in this study on Chaste, as shown in the comparative study in Appendix A. The comparative predictions also validated the need for a proper fiber orientation definition. Therefore, the Holzapfel and Ogden model we herein implemented was essential for the proper investigation of the effects of Na^+ channel blocking drugs on cardiac mechanics.

In particular, the Holzapfel and Ogden model features orthogonal components of energy, calibrated using both shear and biaxial tests that were performed on a cube of passive myocardium tissue. It distinguishes responses in the fiber (**f**), sheet (**s**) and normal (**n**) directions. In it, the strain energy density $W(\mathbf{u})$ is given by,

$$W(\mathbf{u}) = \frac{a}{2b}\exp(b[I_1 - d]) + \sum_{\mathbf{i}=\mathbf{f},\mathbf{s}} \frac{a_{\mathbf{i}}}{2b_{\mathbf{i}}}\left[\exp\left(b_{\mathbf{i}}\left[I_{4,\mathbf{i}} - 1\right]^2\right) - 1\right] + \frac{a_{\mathbf{fs}}}{2b_{\mathbf{fs}}}\exp\left(b_{\mathbf{fs}} I_{8,\mathbf{fs}}^2 - 1\right) \quad [5]$$

where a, $a_{\mathbf{f}}$, $a_{\mathbf{s}}$, $a_{\mathbf{fs}}$, b, $b_{\mathbf{f}}$, $b_{\mathbf{s}}$ and $b_{\mathbf{fs}}$ are material parameters, and $d = 3$ for three-dimensional models. I_1, I_4 and I_8 are invariants of the right Cauchy-Green Strain $\mathbf{C}$. I_1 is the sole isotropic term, considered to characterize the behavior of the non-muscular, non-collagenous part of the tissue (18).

Orientation dependence in equation [5] appears by specifying the I_4 invariants in fiber and sheet directions, according to $I_{4,\mathbf{i}} = \mathbf{i}\cdot\mathbf{C}\cdot\mathbf{i}$, where $\mathbf{i} \in \{\mathbf{f}_0, \mathbf{s}_0\}$ is a unit vector pointing in the corresponding reference direction, defined in the undeformed configuration. The exponential function applied to the fiber ($I_{4,\mathbf{f}}$) and sheet directions ($I_{4,\mathbf{s}}$) is a good reflection of the high stiffening and energy storage behaviors of muscle fibers and connecting collagen fibers, respectively. A coupling invariant ($I_{8,\mathbf{fs}} = \mathbf{f}_0\cdot\mathbf{C}\cdot\mathbf{s}_0$) is also included, for a better account of cardiac tissue in-sheet shearing. Appendix B shows how to obtain the PK2 stress and the corresponding Jacobian from equation [5].

This model can be reduced to a transversely isotropic one by limiting the parameters to only four; *a, b,* a_f and b_f (setting all others to zero). Indeed, in this study these four parameters were selected from a study by Baillargeon et al. (41), which showed improved predictions of blood ejection fractions than using the same model with all eight parameters (38,42).

3 Model Setup

Geometric Model and Mesh

The geometrical model used in this work was derived from Computerized Tomography (CT) scan data (21,22) of the human ventricular chambers. The mesh of the LV and right ventricle (RV) is composed of approximately 238,000 elements. For the electric problem, these elements are linear tetrahedra, which correspond to approximately 50,000 nodes. For the mechanics problem, quadratic elements that avoid pressure instabilities associated with material incompressibility (43) were used, corresponding to approximately 350,000 nodes.

Generating Myofiber Orientations

The mathematical model presented by Potse et al. (30) which is based on the experimental data collected by Streeter et al. (37) was employed to generate fiber and sheet orientations in the walls of our geometric ventricle model. This model accounts for the continuous change of fiber angle through the ventricular wall. The model was built from histological datasets and is known to relate well to the observed physiology of the ventricles. It thus remains to date the most widely used fiber orientation model in cardiac simulations, in spite of its simple form (44). These fiber and sheet directions informed both the electrophysiological and the mechanical problems in this study.

Electro-mechanical Solver

A patch of endocardium tissue where the ventricular electrical excitation begins, highlighted in Figure 2, was stimulated by a current of -10,000 μA, for the duration of 1 ms. For the mechanical model, Dirichlet boundary conditions were applied to a small cluster of nodes at the bottom of the LV apex, fixing them in all 3 directions, leaving the remainder of the mesh to deform freely. The monodomain reaction-diffusion equation (for electrical propagation) was solved for 500 ms, to ensure complete activation and repolarization of the ventricles, i.e. to simulate ventricular behavior over one cardiac cycle. The corresponding solver on Chaste was called with a time step of 0.05 ms. The Ten Tusscher cell model (i.e. ionic flow model) was called with a time-step of 0.01 ms, using the default parameters in Chaste (25). The Kerchoff active stress model was called with a time-step of 0.01 ms, also using default parameters (36). Material parameters used for the passive stress models are listed in Baillargeon et al. (41) for the Holzapfel and Ogden passive stress model, which was developed in C++ and integrated on Chaste as part of this study. The mechanical equations of equilibrium were solved once per ms, since the mechanics evolves more slowly than the electrical signal can propagate.

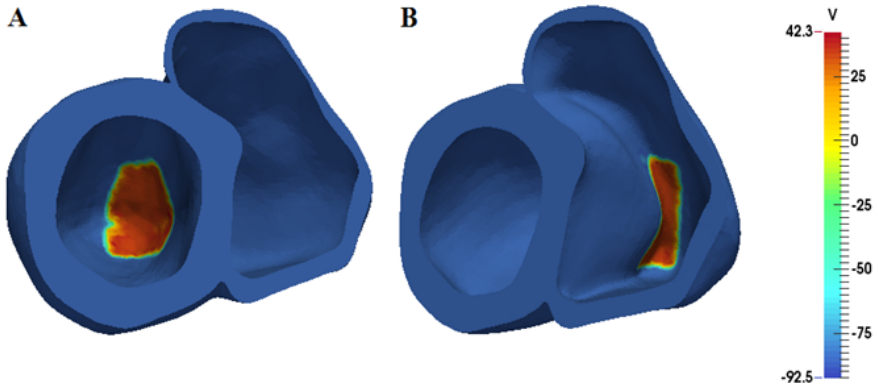

Figure 2: Basal view of ventricular model at time 1 ms highlighting the area of applied stimulus on the endocardium in (A) the left and (B) the right ventricles

Finally, all simulations were performed on an AMD Opteron server with 256 GB of memory, on an Ubuntu 14.04 operating system. Post-processing of the results was performed on *MATLAB*, while mesh visualization, with its electro-mechanical variables, on *Paraview*.

4 Drug Induced Effects

There are two basic ways certain drug molecules can cause ionic flow inhibition when binding to ion channels. The first is when binding occurs near a channel's opening, which results in a physical barrier in the path of ionic flow. The second is a structural change induced in ion channel proteins due to drug binding, which also leads to ionic flow restriction (2). Both cases usually correspond to inhibitory effects on Na^+ channels in myocytes.

For instance, Class I antiarrhythmics, or non-cardiovascular drugs such as antipsychotics and anticonvulsants, can induce Na^+ channel blocks (45). Copper Oxide (CuO) was also found to affect cellular Na^+ concentrations, due to their inhibitory effect on the Na^+ channels (46). Zinc oxide (ZnO) at a concentration of 10-4 g/ml or more has also been shown to activate Na^+ channels and affect intracellular ion concentrations and cell excitability (47). In nanomedicine, literature identifies increased concentrations of silver nanoparticles (AgNPs) to have an inhibitory effect on the Na^+ channel altering cellular electrophysiology (48). Simulations of Na^+ channel blocks thus relate to a multitude of chemical sources and aim to be relevant to the drug development industry.

Electrophysiology

Cardiac electrophysiology is typically accessed via the electrocardiogram (ECG) which records the cardiac electric potential on the body surface. To develop a precise ECG, a solution to the expensive problem of a coupled heart-torso model would be needed. In this work, we instead make an approximation through an averaging scheme for an electrode hypothetically placed at a specified distance from the cardiac domain (22). This approximation produces a pseudo-ECG and a Chaste in-built post-processing tool (23) can be used to calculate it.

A pseudo-ECG for drug-free cardiac conditions (control) of a 500 ms cardiac cycle is shown in Figure 3. Since the model is of the ventricles only, the P-wave representing the electrical activity of the atria at the start of the cycle does not appear in the plot. Instead, the plot is traced from the beginning of a QRS complex to the end of a T-wave (i.e., the QT interval), to assess ventricular activation and repolarization over the cardiac cycle (49).

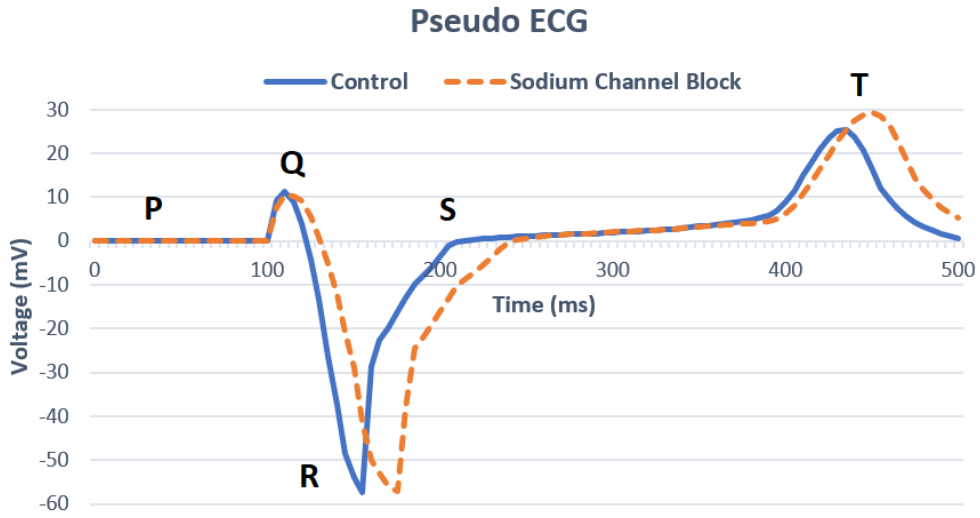

Figure 3: Pseudo-ECG plot of a single cardiac cycle under normal conditions and sodium channel block

Figure 3 superimposes the corresponding pseudo-ECGs predicted for a Na^+ channel blocker which exhibits clear prolongation to its QRS complex, explained by a decreased rate of depolarization. Even though such blockage does not affect repolarization, the T-wave experiences a shift forward as a result of delayed activation. It also causes an increase in the T-wave amplitude. These alterations to the QT interval are consistent with the literature (9,12).

Tissue Mechanics

To model the drug-affected simulations, a 50% Na^+ channel blockage was applied and compared to the control run, in terms of the predicted mechanical biomarkers. We note that Na^+ channel blockers cause depolarization delay (9). Hence, drug-induced mechanical differences are expected to be pronounced at the beginning of an affected cardiac cycle (at ventricular contraction) with Na^+ channel blockers. To quantify such cardiac mechanical differences, several clinically relevant biomarkers are here investigated: 1) LV torsion, 2) LV basal circumferential strain, 3) ventricular volume change, and 4) blood ejection fraction. The comparative findings based on these biomarkers are discussed next.

1) *Left Ventricle Torsion:*

The LV torsion is the difference between the twist at the ventricle's apex and base during the cardiac cycle. The normal heart LV torsion is about 12º at rest and could reach 25º during

exercise and is measured at the end of the LV ejection period (50). Table 1 shows the clinical range for LV torsion along with the model's prediction under normal conditions and under the influence of Na^+ channel block. The control is found to underpredict the LV torsion while the drug-affected model increases the torsion to within the clinical range. This prediction is new to the literature and as yet unexplained.

Table 1: LV Torsion for normal clinical range, control model and Na^+ channel blocked model

Clinical Range	Control	Na^+ Channel Block
~12º - 25º	~10º	~13º

2) Left Ventricle Basal Circumferential Strain:

Advances in speckle-tracking echocardiography and magnetic resonance imaging have enabled strain measures to be used as clinical indicators of cardiac change in dimensions and thus left ventricular functional assessment **(51)**. Table 2 shows the LV circumferential strain measured at the ventricle base for the normal clinical range, the model control predictions and the Na^+ channel block model prediction.

Table 2: LV basal circumferential strain for normal clinical range, control model and Na^+ blocked model

Clinical Range	Control	Na^+ Channel Block
-21 to -28%	-32%	-31.5%

The model over-predicts the clinical strain measure which can be explained by the fact that the deformation at the base of the ventricles should be limited by their attachment to the atria, which are not included in this model. The Na^+ channel block model exhibits slightly less strain with about 20 ms delay from the control consistent with the delay in volume change. Moreover, the LV circumference of the Na^+ channel block model does not recover by the end of the simulation indicating that the block leads to a longer cardiac cycle.

3) Ventricular Volume:

At each time step an irregular-shaped volume is enclosed by the left and right ventricles. This volume is accurately calculated using alpha-volumes, as implemented in *MATLAB* (52). The volumes of the left and right ventricles are plotted in Figure 4 under normal conditions and under the influence of a Na^+ channel blocker. Even though the HO model somewhat under predicts the minimum systolic volume, which could reach as low as 24 cm^3 for the LV and 40 cm^3 for the RV, the trends are very similar to clinical volume change. The Na^+ channel blocked model falls behind the control in left and right ventricle volume evolution. This lag not only affected the contractile phase, but also volume restoration. Hence, the cardiac mechanical cycle has been

prolonged as a result of Na^+ channel blockage and associated activation time delay predicted by the electrophysiology (11,12,51).

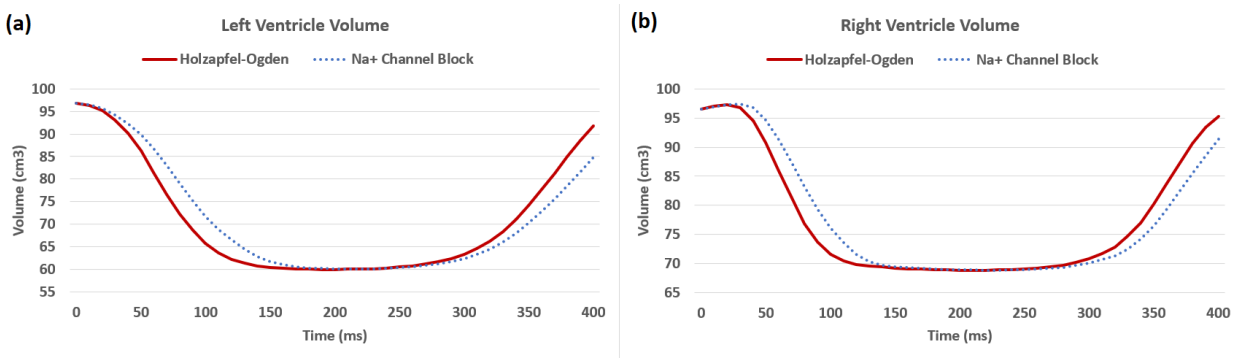

Figure 4: Volume change through time of (a) LV and (b) RV for control model and Na^+ channel blocked model

4) Ejection Fraction:

The ejection fraction (EF) is the percentage of blood ejected from the ventricles during contraction. It is a very good indicator of how healthy the heart is, by virtue of how well it pumps blood. It is calculated from the formula (53);

$$\mathrm{EF} = 100\left(\frac{\mathrm{EDV}-\mathrm{ESV}}{\mathrm{EDV}}\right), \qquad [6]$$

where EDV is the end diastolic volume and ESV is the end systolic volume. The normal range of EFs obtained from the Magdi Yacoub Aswan Heart Center (AHC), the control values produced by the HO model and the predicted EFs for Na^+ channel block are listed in Table 3. It is clear that the values produced by the model are below the clinical range but looking at the effect of the Na^+ channel block on EFs compared to the model control, it is found to be very mild. Hence, we have found no evidence in our study that these blockers can significantly influence EFs. We have been unable to find reports in the literature to compare with our predictions.

Table 3: EF values for the normal clinical range, the control model and the Na^+ channel blocked model

Clinical Range		Control		Na^+ Channel Block	
LV	RV	LV	RV	LV	RV
56 - 78%	47 - 74%	38%	28.79%	37.91%	28.77%

5 Conclusion

This study modeled on the multiphysics solver Chaste a ventricular contraction-relaxation cycle that incorporate an improved passive stress model (Holzapfel and Ogden model), to investigate the electromechanical effects induced by Na^+ ion channel blocking drugs. Our implementation of the Holzapfel and Ogden passive model was used after it was compared to the transverse isotropic Pole-Zero model and the isotropic Mooney-Rivlin model under control

conditions (no drugs) to establish its advantages in cardiac electromechanical modeling where it exhibited the least stiff mechanical response of the three models.

A 50% Na^+ channel block was applied on the ventricular model and its electromechanical effects investigated within the coupled multiphysics framework. Our predictions indicate that a delay in the electrical activation of ventricular tissue caused by a Na^+ channel blocker translates to a delay in the ventricular contraction indicated by the investigation of the LV volume change through time. There was also a cumulative delay effect on the ventricular muscle's return to its relaxed state, prior to the next depolarization cycle. Other than the time delay, there was no significant impact of the drug induced model on the EF or the basal circumferential strain when compared to the control model. However, the Na^+ channel block was found to increase left ventricular twist. Clinical verification of this prediction would be of interest for future work.

Future work will also consider implementing an active stress model that can unveil additional dependency on ionic concentrations, e.g. (54), to further investigate the mechanical effects of K^+ and Ca^{2+} channel blockage, as well as combined channel block effects.

Acknowledgements— The authors gratefully acknowledge EuropeAid for supporting this project under its Scheme 2 Innovation-related action, grant no. RDI2/S2/189. They also acknowledge the Magdi Yacoub Aswan Heart Center (AHC) for providing clinical validation data. This work is based on Master of Science thesis by Noha Shalaby (55).

References

1. Grant AO. Cardiac ion channels. Circ Arrhythmia Electrophysiol. 2009;2(2):185–94.
2. Brennan T, Fink M, Rodriguez B. Multiscale modelling of drug-induced effects on cardiac electrophysiological activity. Eur J Pharm Sci. 2009;36(1):62–77.
3. Piccini JP, Whellan DJ, Berridge BR, Finkle JK, Pettit SD, Stockbridge N, et al. Current challenges in the evaluation of cardiac safety during drug development: Translational medicine meets the Critical Path Initiative. Am Heart J [Internet]. 2009;158(3):317–26.
4. Raschi E, Vasina V, Ursino MG, Boriani G, Martoni A, de Ponti F. Anticancer drugs and cardiotoxicity: Insights and perspectives in the era of targeted therapy. Pharmacol Ther [Internet]. 2010;125(2):196–218.
5. Leifert A, Pan Y, Kinkeldey A, Schiefer F, Setzler J, Scheel O, et al. Differential hERG ion channel activity of ultrasmall gold nanoparticles. Proc Natl Acad Sci U S A [Internet]. 2013;110(20):8004–9.
6. Sarazan RD, Mittelstadt S, Guth B, Koerner J, Zhang J, Pettit S. Cardiovascular function in nonclinical drug safety assessment: current issues and opportunities. Int J Toxicol. 2011;30(3):272–86.
7. Trayanova N a, Constantino J, Gurev V. Electromechanical models of the ventricles. Am J Physiol Heart Circ Physiol. 2011;301(2):H279–86.
8. Sahli Costabal F, Yao J, Kuhl E. Predicting drug-induced arrhythmias by multiscale modeling. Int j numer method biomed eng. 2018;34(5):1–15.
9. Zemzemi N, Bernabeu MO, Saiz J, Rodriguez B. Simulating drug-induced effects on the heart: From ion channel to body surface electrocardiogram. Lect Notes Comput Sci (including Subser Lect Notes Artif Intell Lect Notes Bioinformatics). 2011;6666 LNCS:259–66.
10. Zemzemi N, Rodriguez B. Effects of L-type calcium channel and human ether-a-go-go related gene blockers on the electrical activity of the human heart: a simulation study. Europace [Internet]. 2014;17(2):326–33.

11. Zemzemi N, Bernabeu MO, Saiz J, Cooper J, Pathmanathan P, Mirams GR, et al. Computational assessment of drug-induced effects on the electrocardiogram: From ion channel to body surface potentials. Br J Pharmacol. 2013;168(3):718–33.
12. Wilhelms M, Rombach C, Scholz EP, Dossel O, Seemann G. Impact of amiodarone and cisapride on simulated human ventricular electrophysiology and electrocardiograms. Europace [Internet]. 2012;14(suppl 5):v90–6.
13. Trayanova N a., Rice JJ. Cardiac electromechanical models: From cell to organ. Front Physiol. 2011;2 AUG(August):1–19.
14. Göktepe S, Kuhl E. Electromechanics of the heart: A unified approach to the strongly coupled excitation-contraction problem. Comput Mech. 2010;45(2–3):227–43.
15. Rüssel IK, Götte MJW, Bronzwaer JG, Knaapen P, Paulus WJ, van Rossum AC. Left Ventricular Torsion. An Expanding Role in the Analysis of Myocardial Dysfunction. JACC Cardiovasc Imaging [Internet]. 2009;2(5):648–55.
16. Evangelista a., Nardinocchi P, Puddu PE, Teresi L, Torromeo C, Varano V. Torsion of the human left ventricle: Experimental analysis and computational modeling. Prog Biophys Mol Biol [Internet]. 2011;107(1):112–21.
17. Nash MP, Hunter PJ. Computational Mechanics of the Heart. J Elast. 2001;61:113–41.
18. Holzapfel G a, Ogden RW. Constitutive modelling of passive myocardium: a structurally based framework for material characterization. Philos Trans A Math Phys Eng Sci. 2009;367(1902):3445–75.
19. Lee LC, Genet M, Dang AB, Ge L, Guccione JM, Ratcliffe MB. Applications of computational modeling in cardiac surgery. J Card Surg. 2014;29(3):293–302.
20. Collins T a, Bergenholm L, Abdulla T, Yates JWT, Evans N, Chappell MJ, et al. Modeling and Simulation Approaches for Cardiovascular Function and Their Role in Safety Assessment. 2015;(September 2014):1–14.
21. Wallman M, Smith NP, Rodriguez B. Computational methods to reduce uncertainty in the estimation of cardiac conduction properties from electroanatomical recordings. Med Image Anal [Internet]. 2014;18(1):228–40.
22. Bernabeu MO, Wallman M, Rodr B. Shock-Induced Arrhythmogenesis in the Human Heart : a Computational Modelling Study. 2010;760–3.
23. Mirams GR, Arthurs CJ, Bernabeu MO, Bordas R, Cooper J, Corrias A, et al. Chaste: An Open Source C++ Library for Computational Physiology and Biology. PLoS Comput Biol. 2013;9(3).
24. Pathmanathan P, Whiteley JP. A numerical method for cardiac mechanoelectric simulations. Ann Biomed Eng. 2009;37(5):860–73.
25. Tusscher KHWJ Ten, Panfilov A V. Cell model for efficient simulation of wave propagation in human ventricular tissue under normal and pathological conditions. 2006;51:6141–56.
26. Bernabeu MO, Southern J, Wilson N, Strazdins P, Cooper J, Pitt-Francis J. Chaste: a case study of parallelisationof an open source finite-elementsolver with applications tocomputational cardiacelectrophysiology simulation. Int J High Perform Comput Appl [Internet]. 2013;28(1):13–32.
27. Grandi E, Pasqualini FS, Bers DM. A novel computational model of the human ventricular action potential and Ca transient. J Mol Cell Cardiol. 2010;48(1):112–21.
28. Richardson ES, Xiao Y. Cardiac Electrophysiology Methods and Models. Business [Internet]. 2010;329–48.
29. Sundnes J, Lines G, Cai X, Nielsen B. Computing the electrical activity in the heart. 2007.
30. Potse M, Dube B, Richer J, Vinet A, Gulrajani RM. A Comparison of Monodomain and Bidomain Reaction-Diffusion Models for Action Potential Propagation in the Human Heart. IEEE Trans Biomed Eng [Internet]. 2006 Dec;53(12):2425–35.
31. Dirichlet A, Pde C. Chaste : Finite Element Implementations. Article. 2011;1–22.
32. Palit A, Bhudia SK, Arvanitis TN, Turley GA, Williams MA. Computational modelling of left-ventricular diastolic mechanics: Effect of fibre orientation and right-ventricle topology. J Biomech [Internet]. 2015 Feb;48(4):604–12.

33. Sengupta PP, Tajik a. J, Chandrasekaran K, Khandheria BK. Twist Mechanics of the Left Ventricle. Principles and Application. JACC Cardiovasc Imaging. 2008;1(3):366–76.
34. van Dalen BM, Geleijnse ML. Left Ventricular Twist in Cardiomyopathy. In: Cardiomyopathies [Internet]. InTech; 2013.
35. Kandel ER, Schwartz JH, Jessell TM. Principles of neural science. Vol. 4. New York: McGraw-Hill. 2000.
36. Kerckhoffs RCP, Bovendeerd PHM, Kotte JCS, Prinzen FW, Smits K, Arts T. Homogeneity of cardiac contraction despite physiological asynchrony of depolarization: A model study. Ann Biomed Eng. 2003;31(5):536–47.
37. Streeter DD, Spotnitz HM, Patel DP, Ross J, Sonnenblick EH. Fiber orientation in the canine left ventricle during diastole and systole. Circ Res. 1969;24(3):339–47.
38. Rossi S, Ruiz-Baier R, Pavarino LF, Quarteroni A. Orthotropic active strain models for the numerical simulation of cardiac biomechanics. Int j numer method biomed eng [Internet]. 2012 Jun;28(6–7):761–88.
39. Mooney M. A theory of large elastic deformation. J Appl Phys. 1940;11(9):582–92.
40. Rivlin RS. Large Elastic Deformations of Isotropic Materials . I. Fundamental Concepts. Philos Trans R Soc London Ser A, Math Phys Sci. 1948;240(822):459–90.
41. Baillargeon B, Costa I, Leach JR, Lee LC, Genet M, Toutain A, et al. Human Cardiac Function Simulator for the Optimal Design of a Novel Annuloplasty Ring with a Sub-valvular Element for Correction of Ischemic Mitral Regurgitation. Cardiovasc Eng Technol [Internet]. 2015.
42. Baillargeon B, Rebelo N, Fox DD, Taylor RL, Kuhl E. The Living Heart Project: A robust and integrative simulator for human heart function. Eur J Mech A/Solids [Internet]. 2014;48:38–47.
43. Gartling DK, Dohrmann CR. Quadratic finite elements and incompressible viscous flows. Comput Methods Appl Mech Eng. 2006;195(13–16):1692–708.
44. Lekadir K, Ghafaryasl B, Muñoz-Moreno E, Butakoff C, Hoogendoorn C, Frangi AF. Predictive modeling of cardiac fiber orientation using the knutsson mapping. Lect Notes Comput Sci (including Subser Lect Notes Artif Intell Lect Notes Bioinformatics). 2011;6892 LNCS(PART 2):50–7.
45. Harmer A, Valentin J-P, Pollard C. On the relationship between block of the cardiac Na + channel and drug-induced prolongation of the QRS complex. Br J Pharmacol [Internet]. 2011 Sep 1;164(2):260–73.
46. Liu Z, Liu S, Ren G, Zhang T, Yang Z. Nano-CuO inhibited voltage-gated sodium current of hippocampal CA1 neurons via reactive oxygen species but independent from G-proteins pathway. J Appl Toxicol. 2011;31(5):439–45.
47. Kumar SA, Chen S. Nanostructured Zinc Oxide Particles in Chemically Modified Electrodes for Biosensor Applications. Anal Lett. 2008;41(December 2013):141–58.
48. Liu Z, Ren G, Zhang T, Yang Z. Action potential changes associated with the inhibitory effects on voltage-gated sodium current of hippocampal CA1 neurons by silver nanoparticles. Toxicology. 2009;264(3):179–84.
49. Dupraz M, Filippi S, Gizzi A, Quarteroni A, Ruiz-Baier R. Finite element and finite volume-element simulation of pseudo-ECGs and cardiac alternans. Math Methods Appl Sci. 2015;38(6):1046–58.
50. Bloechlinger S, Grander W, Bryner J, Dünser MW. Left ventricular rotation: A neglected aspect of the cardiac cycle. Intensive Care Med. 2011;37(1):156–63.
51. Yingchoncharoen T, Agarwal S, Popović ZB, Marwick TH. Normal ranges of left ventricular strain: A meta-analysis. J Am Soc Echocardiogr. 2013;26(2):185–91.
52. http://www.mathworks.com/matlabcentral/fileexchange/28851-alpha-shapes/content/alphavol.m
53. Eriksson T, Prassl A, Plank G, Holzapfel G. Influence of myocardial fiber/sheet orientations on left ventricular mechanical contraction. Math Mech Solids [Internet]. 2013;18(6):592–606.
54. Nickerson D, Smith N, Hunter P. New developments in a strongly coupled cardiac electromechanical model. Europace. 2005;7(SUPPL. 2):118–27.
55. Shalaby NM. Computational modeling of nanodrug-induced effects on cardiac electromechanics. MSc Thesis, American University in Cairo, Egypt, 2016.

Appendix A

Passive Stress Model Comparison

Our implementation of the Holzapfel and Ogden (HO) model was run under the same conditions and compared against the Pole-Zero (PZ) and the Mooney-Rivlin (MR) models. Side-by-side maps are shown in Figure A1, for deformed cardiac tissue at mid-cycle, as predicted by the HO, the PZ and the MR models. The maps are colored by effective deviatoric PK2 stress ($T'_{eff} = \sqrt{\frac{3}{2}\mathbf{T}':\mathbf{T}'}$) predicted at mid-cycle. The PZ model clearly exhibits higher stress levels than the HO model for comparable deformation, specifically in the left ventricular tissue, which indicates stiffer cardiac tissue behavior from the PZ model. The MR model exhibits the highest effective stresses and least deformation across the cardiac domain, thus features even stiffer cardiac tissue.

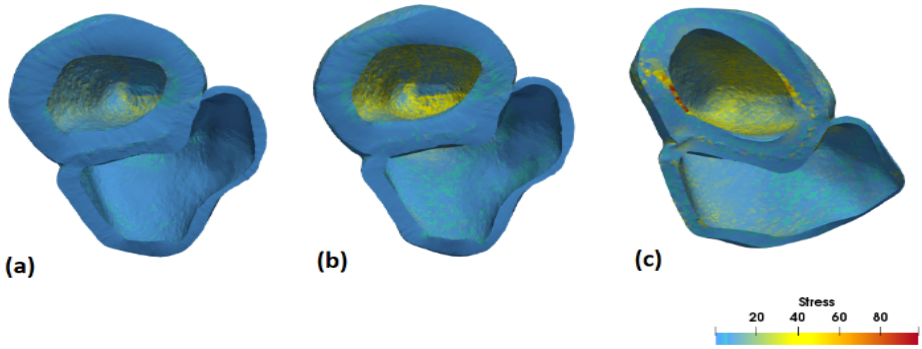

Figure A1: Effective deviatoric PK2 stress maps mid-cycle in kPa for (a) Holzapfel and Ogden Model, (b) Pole-Zero Model, (c) Mooney-Rivlin Model

Both the MR and PZ models are thus expected to under-predict the mechanical function of the ventricles for a cardiac cycle, compared to the newly implemented HO model. To further quantify such cardiac mechanical function ventricular volume change and blood ejection fraction were investigated. These comparative findings based on these biomarkers are discussed next.

Ventricular volume: Figure A2 plots the current volume of the left and right ventricles for a cardiac cycle, as predicted by the three models and relevant volume information is summarized in Table A1. As indicated in Table AI, of all three passive models, the HO model predicts the strongest ventricular contraction for the given electrical excitation, which is desirable. Nonetheless, all three models under predict minimum systolic volumes, which should reach as low as 24 cm^3 for the LV and 40 cm^3 for the RV.

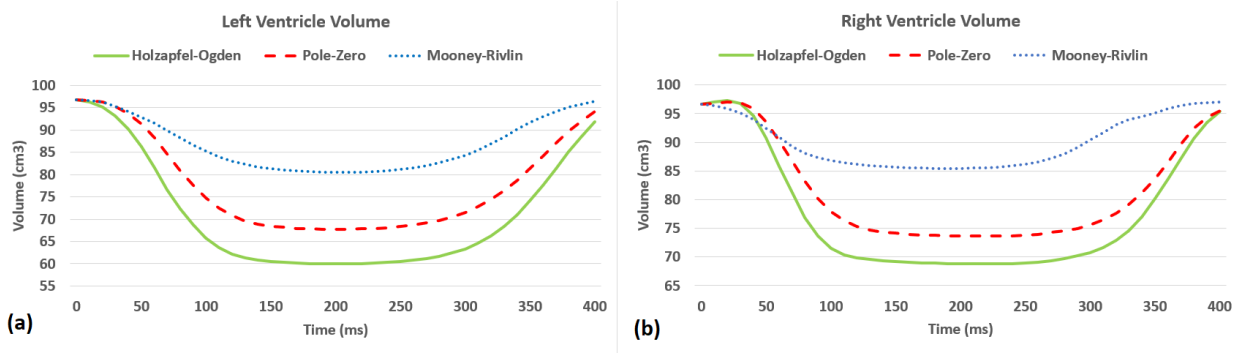

Figure A2: Current volume plot over a cardiac cycle for (a) LV and (b) RV, according to the three passive models

Ejection Fraction: The values of the ejection fraction (EF) predicted by the HO, the PZ and the MR models are shown in Table A1. As expected, the HO model exhibits a larger EF than either the PZ or the MR model, due to the larger change in volume. While these values remain smaller than clinical data, they are consistent with the various computational models in the literature (41) and are thus deemed sufficient for our purpose of detecting the change in a heart's performance under drug influence. In particular, the newly implemented HO model provides a considerable improvement to the ones on the multiphysics solver Chaste.

Table A1: Summary of the LV and RV volumes and ejection fraction values for the three passive models

Passive Model	Initial Volume (cm3)		Minimum Volume (cm3)		Ejection Fraction	
	LV	RV	LV	RV	LV	RV
HO	96.7	96.6	59.9	68.8	38.1%	28.8%
PZ	96.7	96.6	67.7	73.6	29.9%	23.8%
MR	96.7	96.6	80.5	85.4	16.8%	11.6%

Appendix B

The derivative of the energy function W with respect to C is taken to obtain the PK2 stress, T(C, p), with

$$\mathbf{T} = 2\frac{\partial W(\mathbf{u})}{\partial \mathbf{C}} - p\mathbf{C}^{-1} \quad [B1]$$

yielding;

$$\begin{aligned}\frac{\partial W(\mathbf{u})}{\partial \mathbf{C}} &= \frac{a}{2}\exp(b(I_1-3))\mathbf{I} \\ &+a_{\mathbf{f}}(I_{4,\mathbf{f}}-1)\exp(b_{\mathbf{f}}(I_{4,\mathbf{f}}-1)^2)\mathbf{f}_0\otimes\mathbf{f}_0 \\ &+a_{\mathbf{s}}(I_{4,\mathbf{s}}-1)\exp(b_{\mathbf{s}}(I_{4,\mathbf{s}}-1)^2)\mathbf{s}_0\otimes\mathbf{s}_0 \\ &+a_{\mathbf{fs}}I_{8,\mathbf{fs}}\exp(b_{\mathbf{fs}}I_{8,\mathbf{fs}}^2-1)\mathbf{f}_0\otimes\mathbf{s}_0\end{aligned} \quad [B2]$$

where **I** is the identity tensor.

When this model is setup for implicit finite element solvers, the corresponding Jacobian (iteration matrix) is needed and we derive it in this work as follows;

$$\begin{aligned}\frac{1}{4}\frac{\partial \mathbf{T}}{\partial \mathbf{E}} = \frac{\partial \mathbf{T}}{\partial \mathbf{C}} = \frac{a}{2}b\exp\big(b(I_1-3)\big)\mathbf{I}\otimes\mathbf{I} \\ + \left(2b_{\mathbf{f}}\left(I_{4,\mathbf{f}}-1\right)^2+1\right)\left(a_{\mathbf{f}}\exp\left(b_{\mathbf{f}}\left(I_{4,\mathbf{f}}-1\right)^2\right)\right(\mathbf{f}_0\otimes\mathbf{f}_0\otimes\mathbf{f}_0\otimes\mathbf{f}_0) \\ + \left(2b_{\mathbf{s}}\left(I_{4,\mathbf{s}}-1\right)^2+1\right)\left(a_{\mathbf{s}}\exp\left(b_{\mathbf{s}}\left(I_{4,\mathbf{s}}-1\right)^2\right)\right)(\mathbf{s}_0\otimes\mathbf{s}_0\otimes\mathbf{s}_0\otimes\mathbf{s}_0) \\ + \left(2b_{\mathbf{fs}}I_{8,\mathbf{fs}}^2+1\right)\left(a_{\mathbf{fs}}\exp\left(b_{\mathbf{fs}}I_{8,\mathbf{fs}}^2-1\right)\right)(\mathbf{f}_0\otimes\mathbf{s}_0\otimes\mathbf{f}_0\otimes\mathbf{s}_0) + p\mathbf{C}^{-1}\boxtimes\mathbf{C}^{-1}\end{aligned} \quad [B3]$$

where E is the Green-Lagrange strain tensor and is the strain measure of choice in Chaste, which employs the total Lagrangian formulation, wherein E is energetically conjugate to PK2 and

$(\mathbf{C}^{-1}\boxtimes\mathbf{C}^{-1})_{ijmn} = \mathrm{C}_{mi}^{-1}\mathrm{C}_{jn}^{-1}$